CrystEngComm

PAPER

View Article Online
View Journal | View Issue

Cite this: *CrystEngComm*, 2022, **24**, 4262

Solid-state fluorescence of a quasi-isostructural polymorphic biphenyl based Michael addition product†

Poonam Deka,[a] Khemnath Patir,[b] Isha Rawal,[c] Shahnaz Ahmed,[a] Smiti Rani Bora,[a] Dhruba Jyoti Kalita,[a] Khaled Althubeiti,[d] Sonit Kumar Gogoi,[a] Parishmita Sarma*[a] and Ranjit Thakuria*[a]

Received 28th March 2022,
Accepted 2nd May 2022

DOI: 10.1039/d2ce00425a

rsc.li/crystengcomm

Polymorphic materials have gained significant attention owing to their fascinating physicochemical properties. Herein, a biphenyl based Michael addition product (compound **A**) with an active methylene group (dimedone) was synthesized. Compound **A** displayed aggregation-induced emission in an ethanol–water system and in the solid state owing to its highly twisted conformation due to two bulky dimedone groups connected to a sp^3 hybridized C atom. It is dimorphic in nature (forms 1 and 2) with the two forms having identical crystal packing densities (the calculated density is 1.201 g cm^{-3}). Form 1 was solved in the $P2_1/c$ monoclinic space group, whereas form 2 was solved in the $P\bar{1}$ triclinic space group. The quasi-isostructural nature of the two polymorphic systems of the synthesized compound resulted in identical photo-physical behaviours.

Introduction

Organic fluorophores displaying variable solid-state fluorescence emission have attracted widespread attention. They have significant applications in the fields of chemical sensors,[1,2] light-emitting diodes,[3] lasers,[4] photovoltaic devices,[5] mechanical sensors[6,7] *etc.* Switchable fluorescence can be achieved using a crystal engineering approach[8–10] by preparing cocrystals,[11] salts, solvates, and amorphous formulations[12] as well as polymorphic phases.[13–18] Among these, mechanofluorochromic as well as polymorphic materials are of utmost importance and have broader application in the design of fluorescence-based sensors.[19–24] Polymorphism is the ability of a solid material to exist in more than one crystalline form. Due to differences in packing arrangement, polymorphic materials show variable physicochemical properties which are of significant importance in designing functional materials, pharmaceutical solids, explosives, dyes, and pigments.[25–27] Some of the polymorphic organic fluorophores studied in the recent literature include substituted benzothiazole-fluorene based materials,[28] triphenylphosphonium fluorenylide,[29,30] 1-acetylpyrene,[31] *N*,*N*-dimethylanilino naphthalimide,[17] *etc.* which show outstanding photo-physical behaviour. Apart from the listed molecules, several polymorphic organic fluorophores have been synthesized by various research groups in the recent past, with distinct properties.[32–39] In a recent highlight, Ito[40] summarizes various luminescent organic polymorphs with mechanoresponsive properties along with pseudopolymorphs and cocrystal polymorphs.

Most of the reported organic fluorophores display high emission in the solution phase whereas they become non-emissive in the solid state due to aggregation-caused quenching (ACQ).[41,42] In 2001, an opposite behaviour to that of ACQ was discovered, known as aggregation-induced emission (AIE).[43] This class of organic molecules shows low emission in the solution phase but high emission in the solid state (crystal/powder/film/aggregation in solution and in the matrix).[44,45] Several mechanisms have been proposed to explain this phenomenon including restricted intramolecular rotation (RIR),[46] the formation of J-type aggregates,[47] and twisted intramolecular charge transfer (TICT).[44] AIE based fluorophores possess a non-planar twisted geometry with rotator and stator building blocks that induce steric hindrance resulting in RIR.[45,48] Tetraphenylethylene, silole, and distyrylanthracene derivatives are a few of them.[44,49–51]

[a] *Department of Chemistry, Gauhati University, Guwahati 781014, India. E-mail: parishmita09@gmail.com, ranjit.thakuria@gmail.com, ranjit.thakuria@gauhati.ac.in*
[b] *Department of Applied Science and Humanities, Assam University, Silchar 788011, India*
[c] *Department of Chemistry, Indian Institute of Science Education and Research Bhopal, Bhopal By-Pass Road, Bhauri, Bhopal, 462066, Madhya Pradesh, India*
[d] *Department of Chemistry, College of Science, Taif University, Taif 21944, Saudi Arabia*

† Electronic supplementary information (ESI) available. CCDC 1993302–1993304. For ESI and crystallographic data in CIF or other electronic format see DOI: https://doi.org/10.1039/d2ce00425a

The factors affecting the optical performance of organic fluorophores include differences in crystal packing, molecular conformations, and intermolecular interactions.[52,53] Subtle modifications in intermolecular interactions such as hydrogen bonding, halogen bonding, π···π interactions, and C–H···π interactions produce a different molecular arrangement and a drastic change in their optoelectronic properties. In a recent report, Sarma *et al.*[54] synthesized a few biphenyl based donor–π–acceptor organic fluorophores that showed AIE along with mechanofluorochromism. As an extension to that, a dimorphic biphenyl based Michael addition product was synthesized. Despite the absence of π-conjugation, bulky dimedone groups induce a twisted conformation of the synthesized compound, resulting in AIE features.

Herein, we reported the synthesis, characterization, and photo-physical properties of an organic fluorophore, compound **A**, based on Michael addition. We observed a counter interfering result *i.e.*, two polymorphic forms of compound **A** with identical photo-physical behaviours. The detailed synthetic procedures are discussed in the experimental section.

Experimental section

Materials

Biphenyl-4-carboxaldehyde and 5,5-dimethylcyclohexane-1,3-dione (dimedone) were purchased from Sigma-Aldrich and used without further purification.

Synthesis of compound A. A round-bottom flask was charged with biphenyl-4-carboxaldehyde (364.44 mg, 2.00 mmol), dimedone (560.72 mg, 4.00 mmol), and 2 mL of polyethyleneglycol (PEG). The mixture was stirred at room temperature or up to 120 °C for 48 h. 2 mL of water was added to the mixture resulting in a white solid precipitate (compound **A**). The precipitate was filtered, washed with water to remove excess PEG, dried off, and purified by recrystallization from ethanol. Block-shaped single crystals of form 1 was obtained from solution crystallization with ethanol solvent. Form 2 was obtained concomitantly during solution crystallization from a 1 : 1 mixture of hexane–tetrahydrofuran (THF) as well as dichloromethane (DCM). Extensive screening by mechanical grinding using various liquids as well as solution crystallization always resulted in the precipitation of the form 1 material. The use of a previously reported[55] porous organic polymer (AmPOP) as the catalyst instead of PEG resulted in the formation of a non-fluorescent xanthine derivative (compound **B**) confirmed using SCXRD (see the ESI†).

Instrumentation

All the absorbance and fluorescence measurements of the samples were recorded on Shimadzu UV-1800, Hitachi F-7000, and Horiba FluoroMax spectrophotometers, respectively. The fluorescence quantum yields of the samples were recorded on a Horiba FluoroMax using an integrating sphere. X-ray reflections were collected on a Bruker SMART APEX II CCD equipped with a graphite monochromator and a Mo Kα fine-focus sealed tube (λ = 0.71073 Å). Data integration was done using SAINT. The intensities for absorption were corrected using SADABS. Structure solution and refinement were carried out using Bruker SHELXTL. The hydrogen atoms were refined isotropically, and the heavy atoms were refined anisotropically. O–H hydrogen atoms were located from difference electron density maps, and C–H hydrogen atoms were fixed using the HFIX command in SHELXTL. Crystallographic files (CIF) are deposited with the CCDC (no. 1993302–1993304). X-ray data are summarized in Table 1. Powder X-ray diffraction (PXRD) measurements of the samples were performed using a Rigaku Ultima IV diffractometer with a CuKα X-ray source and equipped with a Ni filter to suppress K_β emission and a D/teX Ultra-high-speed position sensitive detector, and measurements were performed at room temperature, with a scan range 2θ = 5–50°, a step size of 0.02°, and scan rate of 10° min^{-1}. DSC measurements were performed using a Mettler Toledo DSC 822e module. The typical sample size is 4–10 mg for DSC. Samples were heated at 10 °C min^{-1} in the temperature range of 25–300 °C under an ultra-high purity nitrogen environment purged at 40 mL min^{-1}. HR-MS measurements of compound **A** were carried out using a Waters Xevo G2-XS QTof high-resolution mass spectrometer. ^{1}H and ^{13}C NMR spectra of the samples were measured using a Bruker 300 MHz nuclear magnetic resonance (NMR) spectrometer.

Aggregation induced emission (AIE) experiments

The UV-visible spectrum of compound **A** was recorded in ethanol (1 mM), as shown in Fig. 4a. Compound **A** exhibited absorbance at 265 nm, assigned to the presence of a biphenyl system. Compound **A** was soluble in most of the commonly available organic solvents but insoluble in water. For the aggregation study, compound **A** was first dissolved in ethanol (1 mM) followed by the addition of varying volumes of water to obtain the desired V/V percentage of the mixture solvent system and kept for 30 min at room temperature. After 30 min, the fluorescence spectra of the samples were recorded.

Results and discussion

Herein, we designed and synthesized a Michael addition product, compound **A**, that is dimorphic in nature. The synthesis of compound **A** is summarized and is shown in Scheme 1. The formation of compound **A** was further confirmed using HR-MS and solution NMR (see ESI† Fig. S2 and S3) as well as single crystal X-ray diffraction (SCXRD) analysis.

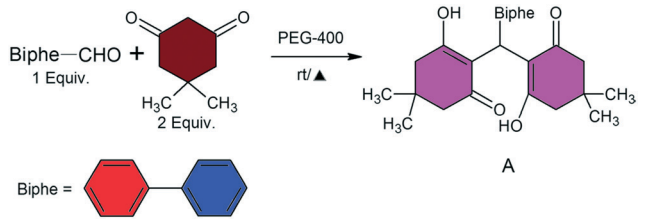

Scheme 1 Synthetic scheme of compound **A**.

Structural analysis

Compound A: form 1. During solution phase crystallization, two polymorphic phases of compound **A** were obtained. A stable form 1 was obtained during solution crystallization from a majority of organic solvents (see Fig. 2a and b), confirmed using SCXRD as well as PXRD analysis. SCXRD measurements showed the unit cell parameters of form 1 to be a = 9.3281 Å, b = 21. 6191 Å, c = 12.2447 Å, β = 95.321°, and V = 2458.7 Å^3 and the compound was solved in the monoclinic space group $P2_1/c$ containing one molecule in the asymmetric unit (see Table 1). The conformation of the biphenyl ring was found to be non-planar with a dihedral angle of 24.39° resulting in inhibition of the π–π stacking interactions. Moreover, due to incorporation of two bulky dimedone units, the biphenyl rings of adjacent molecules were stacked in a head to tail arrangement, confined in between the dimedone rings from both sides. The biphenyl units were well separated with a centroid to centroid distance of ~4.2 Å resulting in a dimeric motif (Fig. 1a and c). In the 3D crystal packing, these aggregated dimers are arranged in an orthogonal fashion, as shown in Fig. 1e.

Table 1 Crystallographic parameters of compound **A** (form 1 and form 2)

	Compound **A**	
Compound name	Form 1	Form 2
Chemical formula	$C_{29}H_{32}O_4$	$C_{29}H_{32}O_4$
Formula wt.	444.54	444.54
Crystal system	Monoclinic	Triclinic
Space group	$P2_1/c$	$P\bar{1}$
T, K	296	296
a, Å	9.3281(6)	9.3146(7)
b, Å	21.6191(15)	11.4763(9)
c, Å	12.2447(9)	12.2711(9)
α, deg	90	95.205(4)
β, deg	95.321(4)	106.911(4)
γ, deg	90	98.262(4)
Z	4	2
V, Å^3	2458.7(3)	1229.77(16)
D_{calc}, gcm^{-3}	1.201	1.201
μ (mm^{-1})	0.079	0.079
Reflns collected	34 223	15 144
Unique reflns	3958	3978
R_1 [$I > 2(I)$]	0.0586	0.0429
wR_2 (all)	0.1536	0.1316
GOF	1.096	1.057
Data collection	Bruker-Apex II	Bruker-Apex II
CCDC no.	1993304	1993302

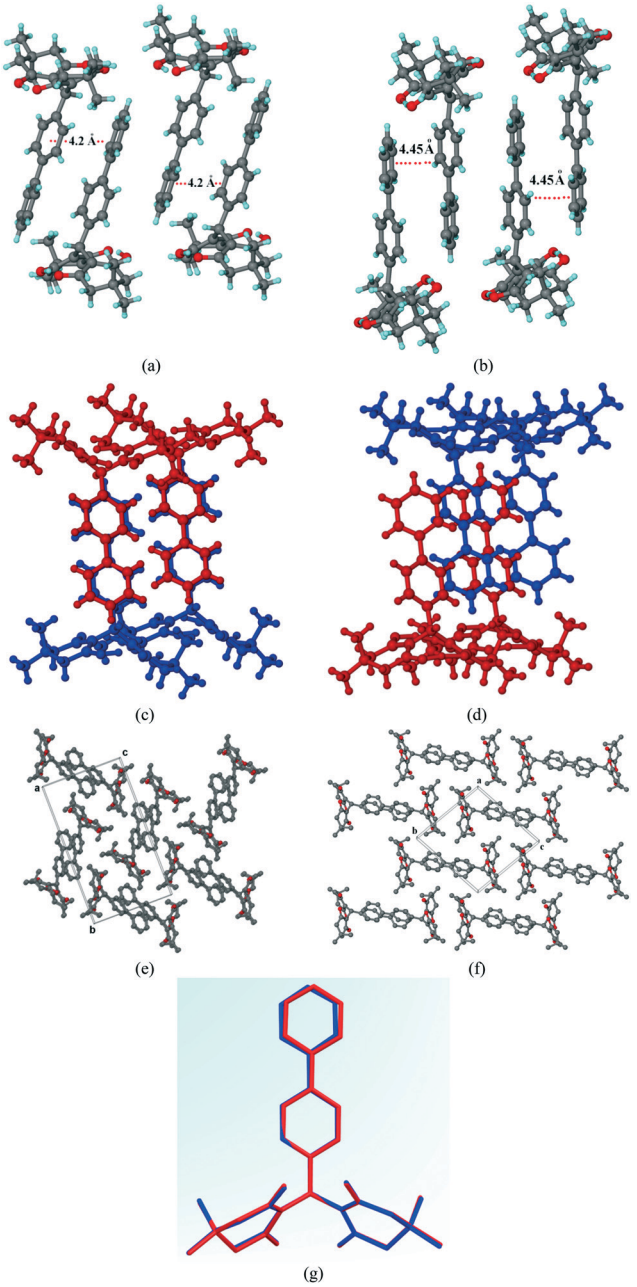

Fig. 1 Head to tail arrangement of molecules with biphenyl centroid to centroid distances shown for (a) form 1 and (b) form 2; stacking arrangements of the dimers in (c) form 1 and (d) form 2; 3D crystal packing arrangements of (e) form 1 and (f) form 2; (g) molecular overlay showing the conformation of the biphenyl ring with respect to the dimedone units in form 1 (red) and form 2 (blue).

Compound A: form 2. Solution crystallization using a 1 : 1 hexane–THF mixture and dichloromethane (DCM) solvent independently resulted in a concomitant mixture of polymorphs (form 1 and form 2) based on SCXRD and PXRD analyses (Fig. 2b). SCXRD measurements show the unit cell parameters to be a = 9.3146 Å, b = 11.4763 Å, c = 12.2711 Å, α = 95.205°, β = 106.911°, γ = 98.262°, and V = 1229.77 Å^3, and the compound was solved in the triclinic space group $P\bar{1}$ containing one molecule in the asymmetric unit. Structural

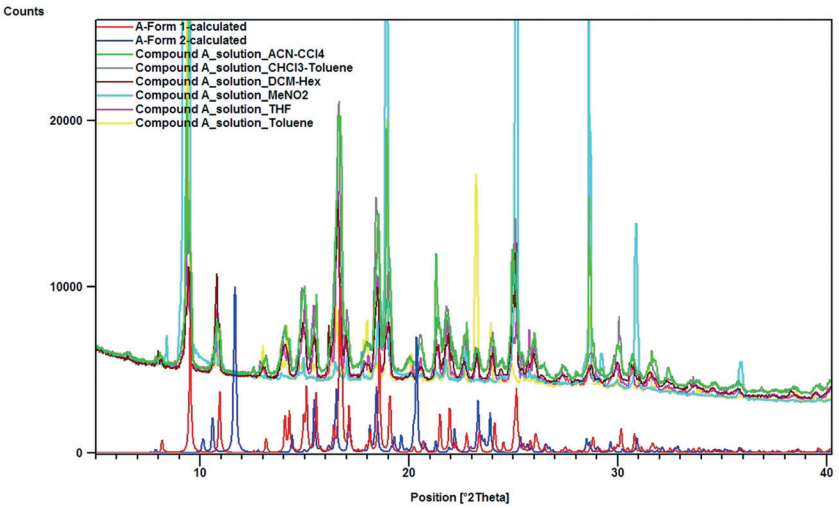

(a)

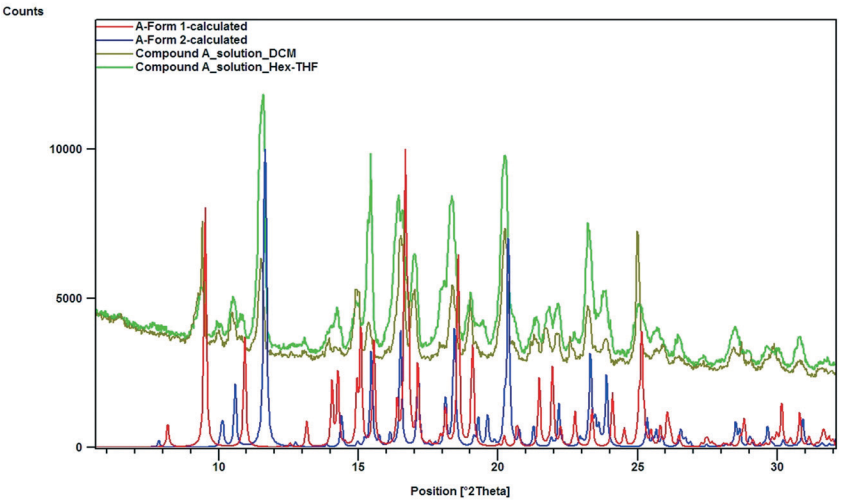

(b)

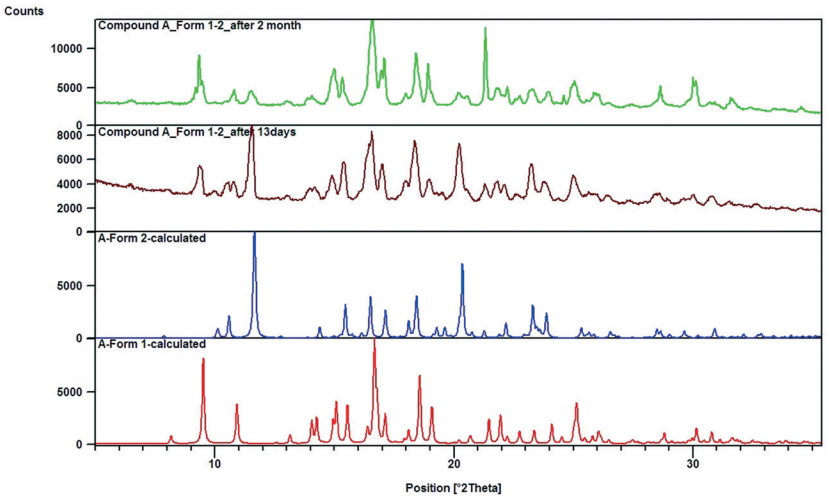

(c)

Fig. 2 (a) PXRD analysis depicting the formation of form 1 upon solution crystallisation in a variety of solvent combinations mentioned; (b) PXRD analysis depicting the formation of form 2 along with form 1 upon solution crystallization independently from DCM and a 1 : 1 mixture of hexane–THF; (c) prolonged storage (ageing) of the concomitant mixture of forms 1 and 2 resulted in slow conversion of the material to form 1 due to the presence of a polymorphic impurity (form 1).

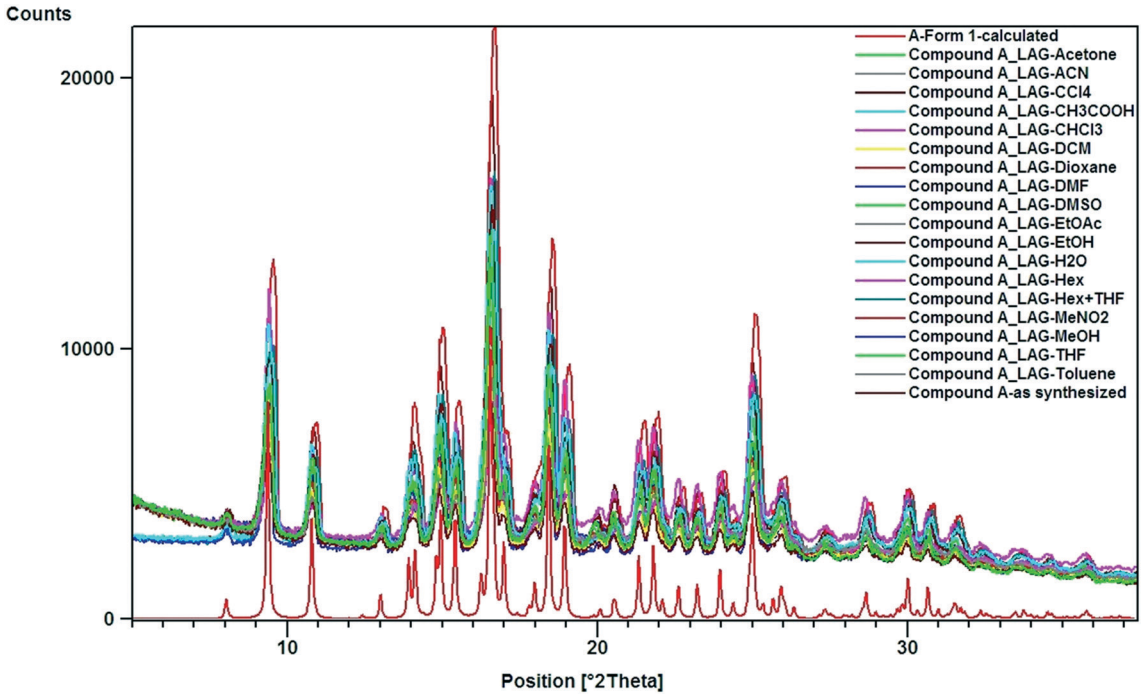

Fig. 3 Experimental PXRD patterns obtained from LAG of compound **A** using various laboratory liquids resulting in the formation of phase pure form 1. Calculated PXRD pattern of form 1 (red) depicting good agreement with the experimental patterns.

analysis showed a slightly offset arrangement of these molecular dimers with a biphenyl centroid to centroid distance of ~4.45 Å, which was slightly higher than that of form 1 with a dihedral angle of 34.15° (Fig. 1b and d). In the 3D crystal packing, these aggregated dimers are aligned along the (011) plane, as shown in Fig. 1f. A clear difference in molecular packing compared to a small change in the biphenyl conformation can be easily visualized from the molecular overlay shown in Fig. 1g. Hence, the two polymorphs can be considered as packing polymorphs. The crystallographic parameters of compound **A** (forms 1 and 2) are listed in Table 1.

An extensive polymorph screening was carried out using both solution crystallization and liquid assisted grinding (LAG). Solution crystallization from most of the laboratory solvents resulted in precipitation of form 1, except for the 1 : 1 mixture of hexane–THF and DCM that yielded a concomitant mixture of forms 1 and 2, confirmed by SCXRD and PXRD measurements (Fig. 2a and b). Although form 2 was obtained concomitantly and had an identical crystal packing density, this polymorph was relatively unstable and slowly converted into form 1 under ambient conditions (25 °C and 60% relative humidity) during the aging experiment, characterized using PXRD (Fig. 2c). The intensity of the 11.6° 2θ peak corresponding to the (011) plane characteristic of form 2 decreased after storage of the powder material for a period of 2 months, whereas the diffraction peaks at 9.5° and 10.9° 2θ corresponding to the (100) and (021) planes, respectively, characteristic of form 1 increased in intensity. The polymorphic impurity (form 1) present in the mixture may act as a molecular seed that initiates phase transformation of form 2 to form 1 as observed from PXRD measurements. Mechanochemical milling of compound **A** with all possible laboratory liquids (LAG) results in the formation of phase pure form 1 based on PXRD analysis (Fig. 3).

Photo-physical study of compound A.‡ The UV-visible and fluorescence spectra of compound **A** in ethanol (1 mM) are shown in Fig. 4a and b. Compound **A** shows an absorbance peak at around 265 nm which is ascribed to the biphenyl unit, similar to the precursors.[56] The ethanolic solution of compound **A** has very low fluorescence with emission centered at 348 nm (Fig. 4b). The observed low fluorescence emission could be attributed to free molecular motion in solution resulting in a high non-radiative decay constant and the electronically non-conjugated nature of compound **A**. Compound **A** was found to aggregate in the ethanol–water mixture at a high water fraction (f_w) due to its hydrophobicity. Increasing the water fraction to above 30% in ethanol resulted in a significant boost of the emission intensity with a red-shift in the emission maxima from 348 to 415 nm (Fig. 5a). The high-intensity red shifted emission peak at 415 nm could be attributed to the formation of molecular aggregates.[57] The plot of fluorescence intensity as a function of water content (%) at λ_{em} = 415 nm (for compound **A**) is shown in Fig. 5b (inset: photograph of

‡ As a polymorphic phase does not exist in solution, all the photo-physical study results correspond to compound **A** and a polymorphic phase was not mentioned during the discussion.

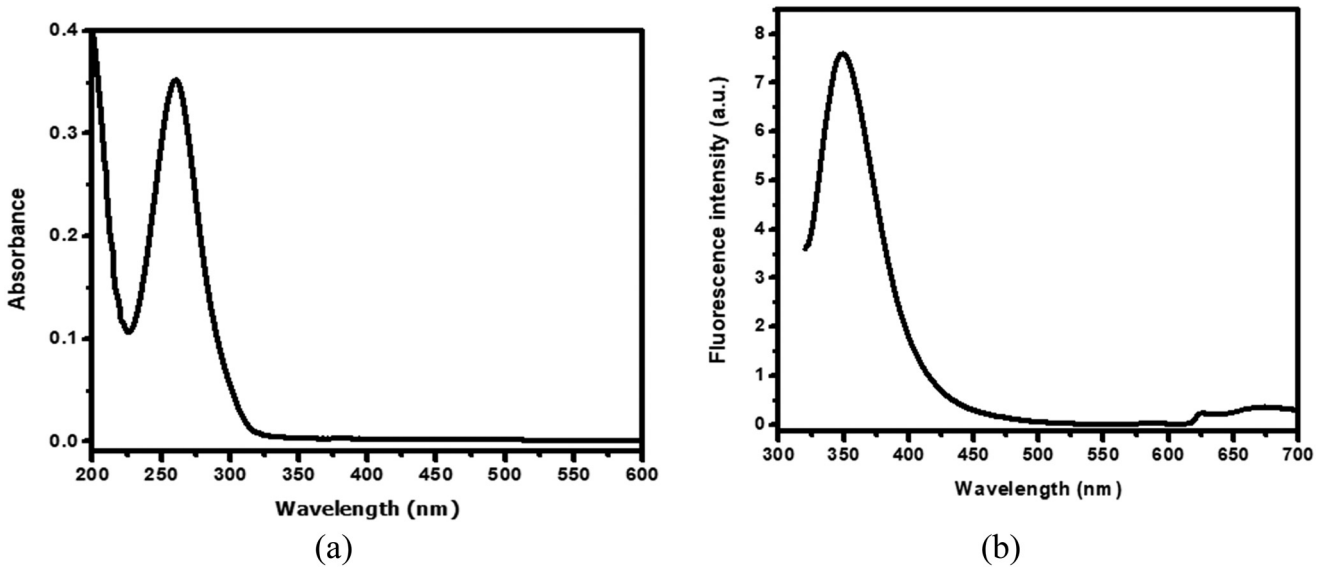

Fig. 4 (a) UV-visible spectrum of compound **A** in ethanol (1 mM) and (b) the corresponding fluorescence spectrum in ethanol (1 mM) under a 310 nm excitation wavelength.

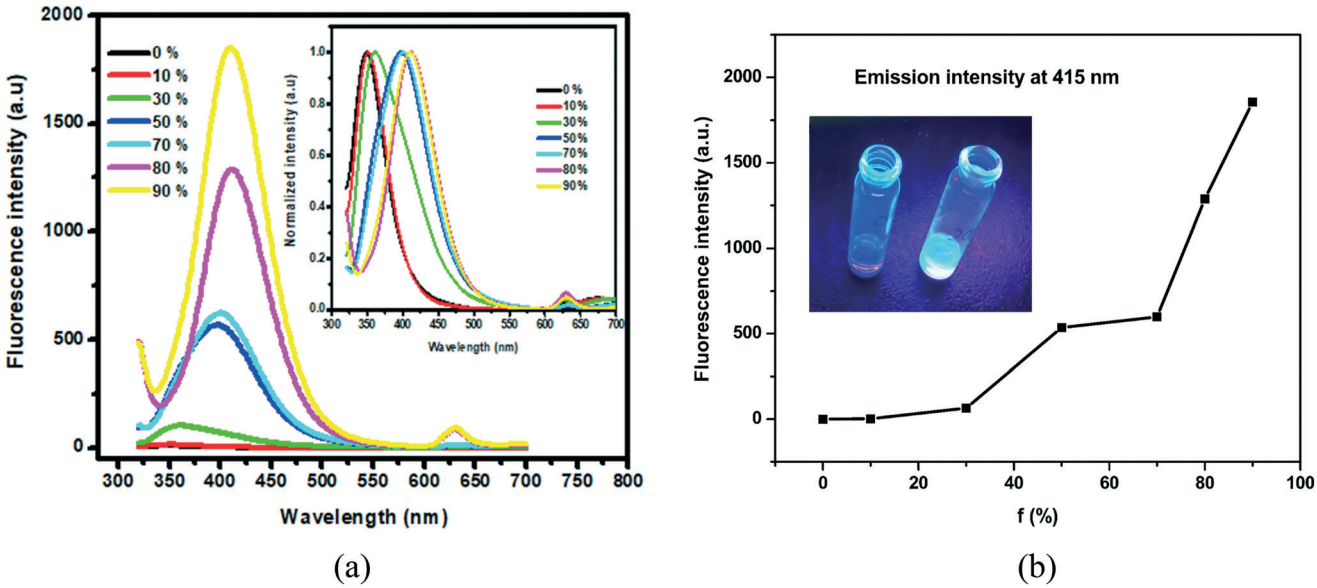

Fig. 5 (a) Fluorescence spectra of compound **A** in ethanol–water with different water percentages (%), f_w (inset: the corresponding normalized spectra) under a 310 nm excitation wavelength; (b) plot of fluorescence intensity at 415 nm with varying percentages of water (%), f_w (inset: the corresponding photographs under daylight and 365 nm UV light irradiation).

compound **A** in ethanol (low fluorescence) and ethanol–water (violet-blue fluorescence)) (f_w = 90%, where f_w is the percentage of water). The fluorescence quantum yields of compound **A** were determined to be 0.00992% and 0.0263%, respectively, in ethanol and in the 90% ethanol–water system based on a standard method,[32] which correlates well with its increasing fluorescence intensity in the mixture solvent system due to the formation of aggregates.

The fluorescence lifetime measurement of compound **A** in ethanolic solution was performed using a 290 nm pulsed diode laser (Fig. 6). The average lifetime of compound **A** was found to be 0.5 ns, confirming the involvement of an excitation–emission process.

In the solid state, both phase pure form 1 and the mixture (forms 1 and 2) of compound **A** displayed fluorescence. The fluorescence spectra of both of these forms were recorded and their emission maxima came out to coincide at 486 nm under a 372 nm excitation wavelength (Fig. 7a and b) (insets: photographs of the two polymorphic forms under daylight and 365 nm UV light). Both forms displayed green fluorescence which could be clearly visualized from the photographs taken under 365 nm UV light irradiation. The

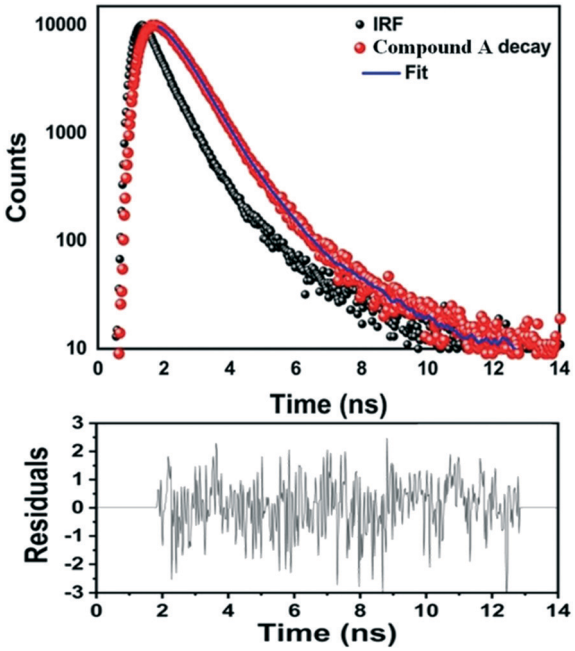

Fig. 6 Fluorescence lifetime decay profile of compound A in ethanolic solution under 290 nm excitation (top) along with the residual fitting, with a χ^2 value of 1.003 (bottom).

presence of a non-planar biphenyl ring and two bulky dimedone units resulted in restricted intramolecular rotation (RIR) of the biphenyl ring thus preventing non-radiative decay. As a consequence, AIE was observed in the solid state, similar to the ethanol–water system (Fig. 5a).[57] In the literature, many reported organic fluorophores exhibited outstanding fluorescence behaviour due to conformational rigidity.[58–60] The fluorescence quantum yields of form 1 and form 1 + 2 of compound **A** were determined to be 1.8% and 0.9%, respectively, by using the integrating sphere method.

In order to understand and quantify the intermolecular interactions present in the two polymorphic systems, Hirshfeld surface analysis and the associated 2D fingerprint plots were generated using Crystal Explorer 3.7.[61,62] As shown in Fig. 8 and Table 2, the relative contributions of the major intermolecular contacts present in both polymorphs are nearly the same. From the Hirshfeld surface analysis, it was observed that both polymorphic forms do not have any strong directional H-bond interactions. The weak C–H···π and van der Waals interactions contribute to the overall crystal packing and they are nearly identical for the two polymorphs.

Energy framework analysis. A comparison of energy frameworks computed for the systematic comparison of the interaction topologies showed a remarkable similarity between the two polymorphs. As both of the polymorphic forms did not posess any strong hydrogen bond interactions, the energy framework of both polymorphs exhibited a 3D network of weakly bound molecules viewed along all three directions (Fig. 9). Interestingly, both electrostatic and dispersion energy frameworks also exhibited similar topologies for forms 1 and 2. Very recently, Chopra and coworkers have reported[63] a dimorphic benzamidamide derivative that showed a quasi-isostructural behaviour based on energy framework analysis. They proposed that a quasi-isostructural polymorph might show similar physical properties; likewise, we also observed near identical photo-physical behaviours for the two polymorphic forms.

Theoretical calculations. All theoretical calculations were performed using the Gaussian 09 program package. The ground state geometries of both forms 1 and 2 of compound **A** were optimized by employing the density functional theory (DFT) method with functional B3LYP and 6-31G(d) basis sets. Moreover, to study the photo-physical properties such as fluorescence emission of the two forms (1 and 2) of

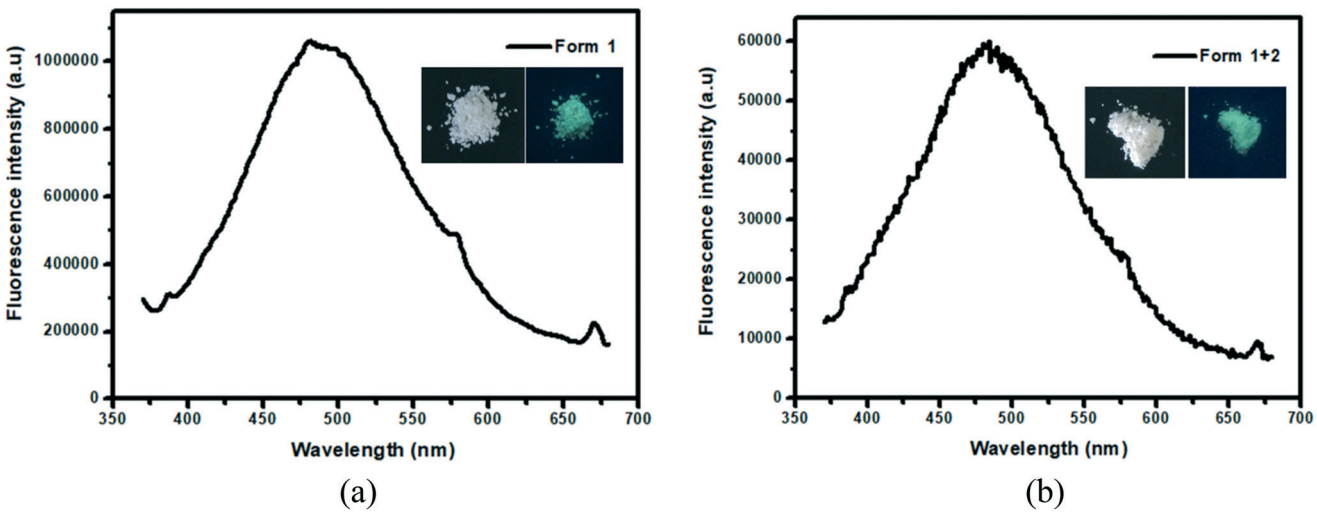

Fig. 7 Solid state fluorescence spectra of (a) form 1 and (b) form (1 + 2) using a 372 nm excitation wavelength (inset: photographs of the two polymorphic forms under daylight and 365 nm UV light).

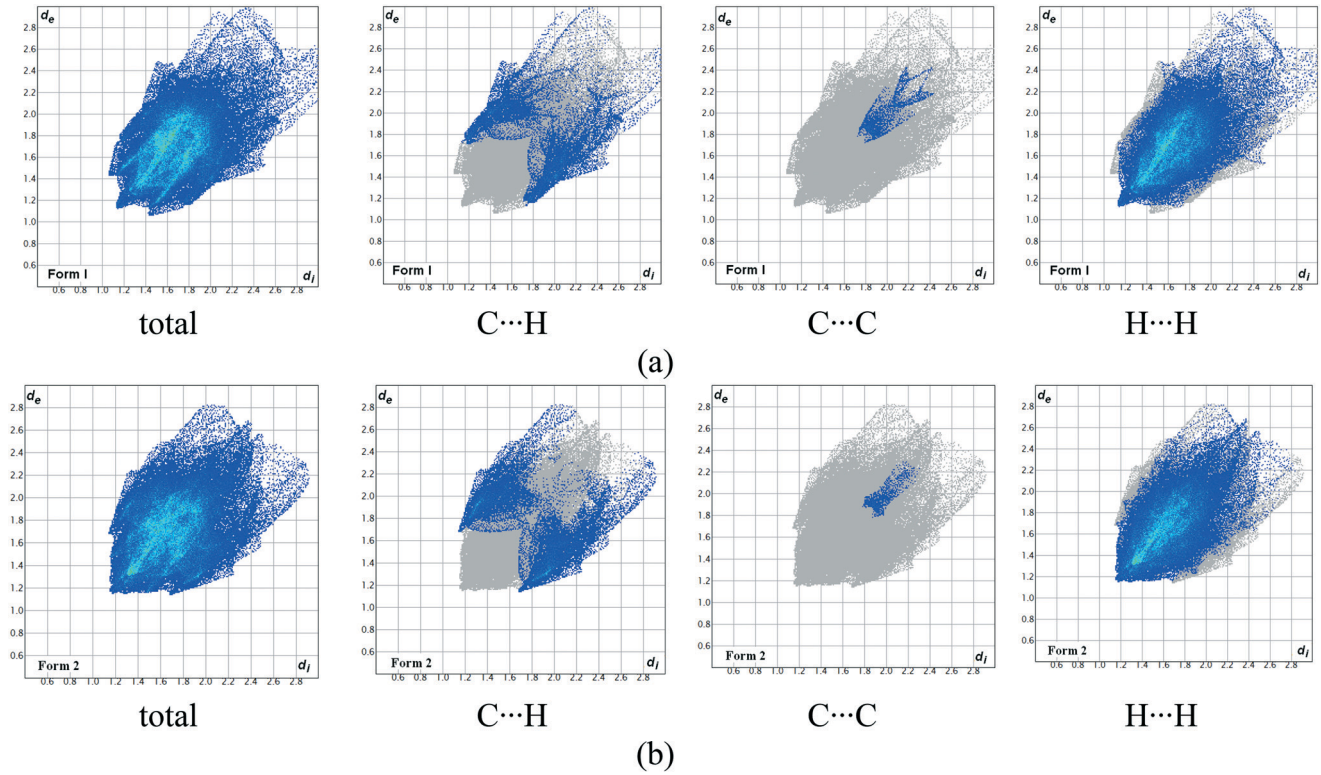

Fig. 8 Hirshfeld fingerprint plots (d_e *vs.* d_i) of compound **A** showing the contributions of individual interactions in (a) form 1 and (b) form 2.

Table 2 Contributions of individual intermolecular interactions to the Hirshfeld surface of forms 1 and 2 of compound **A**

Polymorph	C–H	C–C	H–H	Others
Form 1	14.2	2.2	65.6	18
Form 2	17.5	1.0	63.5	18

compound **A** in the solid phase, we have employed the time-dependent density functional theory (TD-DFT) method at the same level of theory. The fluorescence properties of both forms 1 and 2 of compound **A** have been reported in Table 3 and their optimized molecular HOMO–LUMO structures have been provided in Fig. 10.

From Fig. 10 it was observed that the HOMOs of both forms 1 and 2 are mainly distributed over the biphenyl rings and are partially distributed over the dimedone units. On the other hand, the LUMOs are completely distributed over the dimedone units. Moreover, from Table 3 it is observed that the calculated absorption wavelength of form 2 (calcd. λ_{abs} = 333.69 nm) with an oscillator strength of 0.0021 is significantly shifted in the bathochromic direction relative to that of form 1 (calcd. λ_{abs} = 319.95 nm) whose oscillator strength is 0.0005. Besides, the contribution of charge-transferred HOMO to LUMO transition was observed to be larger for form 1 (0.67264) compared to form 2 (0.56265). The larger value of the contribution of charge-transferred HOMO

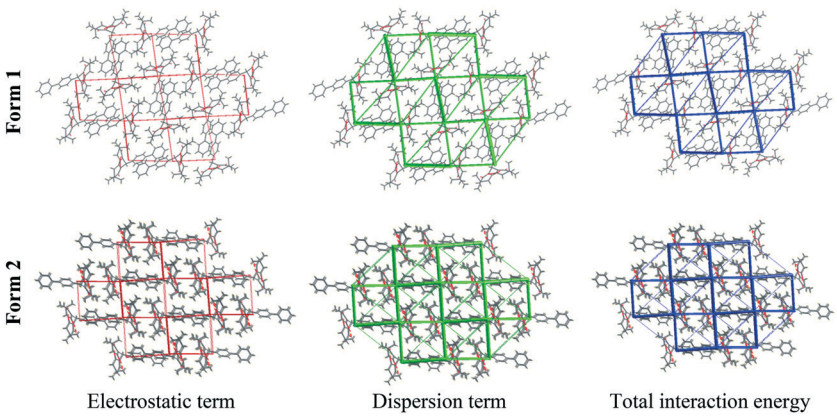

Fig. 9 Energy frameworks corresponding to the electrostatic, dispersion, and net interaction energy components in form 1 and form 2.

Table 3 Fluorescence properties of both forms 1 and 2 of compound A

Compound	Calculated absorption λ_{abs} (nm)	Transition from HOMO to LUMO	Oscillator strength (f_{osc})	HOMO (eV)	LUMO (eV)	Band gap (eV)
Form 1	319.95	0.67264	0.0005	−5.757	−1.305	4.452
Form 2	333.69	0.56265	0.0021	−5.739	−1.464	4.275

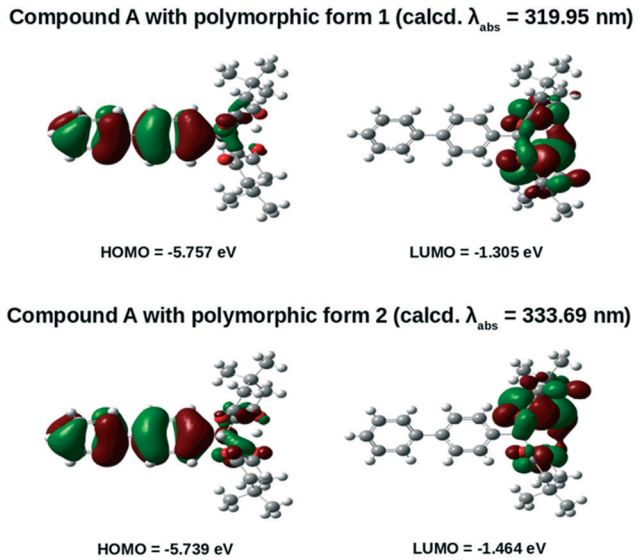

Fig. 10 HOMO and LUMO of forms 1 and 2 of compound A calculated at the B3LYP/6-31G(d) level of theory.

to LUMO transition for compound **A** in polymorphic form 1 might probably be due to its relatively planar structure.

Conclusions

In conclusion, we have synthesized compound **A** that shows solid-state fluorescence as well as AIE behaviour in an ethanol–water system. Compound **A** is dimorphic in nature with the occurrence of a metastable concomitant polymorph. The presence of bulky dimedones and weak C–H···π interactions in compound **A** leads to RIR, resulting in an AIE behaviour which is further confirmed by a photo-physical study. The identical photo-physical behaviours of the two polymorphic systems are attributed to the nearly identical HOMO–LUMO gap and intermolecular interactions present in the crystal structures, as indicated by the DFT calculation. Our findings show that the presence of identical intermolecular interactions along with a quasi-isostructural nature results in similar photo-physical properties for a polymorphic organic fluorophore.

Conflicts of interest

The authors declare no competing financial interests.

Acknowledgements

P. D. thanks UGC for Junior Research Fellowship (JRF), P. S. is grateful to the Science and Engineering Research Board (SERB) DST-NPDF scheme (Project No. PDF/2017/000126) for financial support. K. A. thanks the Taif University Researchers Supporting Project (TURSP-2020/241), Taif University, Taif, Saudi Arabia. S. K. G. thanks the SERB-DST (SB/S1/PC-105/2012) for financial assistance. S. R. B. thanks MOTA for Junior Research Fellowship (JRF). D. J. K. would like to acknowledge the DST-SERB (SB/FT/CS-077/2013) and UGC-BSR (NO.F.30.-122/2015(BSR) for providing financial assistance. R. T. thanks the Science and Engineering Research Board for funding under the Teachers Associateship for Research Excellence (TARE) grant (Project No. TAR/2021/000251). We thankfully acknowledge the Sophisticated Analytical Instrumentation Facility (SAIF), GU for the provision of the single crystal X-ray diffractometer and the Department of Chemistry, GU for the Rigaku powder X-ray diffractometer, basic instrumentation facility, and infrastructure. We thank Prof. Abhijit Patra of the Indian Institute of Science Education and Research Bhopal for helping us with fluorescence measurements and fruitful discussions.

References

1 D. Yan, J. Lu, J. Ma, M. Wei, D. G. Evans and X. Duan, Reversibly Thermochromic, Fluorescent Ultrathin Films with a Supramolecular Architecture, *Angew. Chem., Int. Ed.*, 2011, **50**, 720–723.

2 D. Sharada, A. Saha and B. K. Saha, Charge transfer complexes as colour changing and disappearing–reappearing colour materials, *New J. Chem.*, 2019, **43**, 7562–7566.

3 C. A. Strassert, C.-H. Chien, M. D. Galvez Lopez, D. Kourkoulos, D. Hertel, K. Meerholz and L. De Cola, Switching On Luminescence by the Self-Assembly of a Platinum(II) Complex into Gelating Nanofibers and Electroluminescent Films, *Angew. Chem., Int. Ed.*, 2011, **50**, 946–950.

4 Y. Liu, C. Li, Z. Ren, S. Yan and M. R. Bryce, All-organic thermally activated delayed fluorescence materials for organic light-emitting diodes, *Nat. Rev. Mater.*, 2018, **3**, 18020.

5 S. J. Kang, S. Ahn, J. B. Kim, C. Schenck, A. M. Hiszpanski, S. Oh, T. Schiros, Y.-L. Loo and C. Nuckolls, Using Self-Organization To Control Morphology in Molecular Photovoltaics, *J. Am. Chem. Soc.*, 2013, **135**, 2207–2212.

6 R. Göstl and R. P. Sijbesma, π-extended anthracenes as sensitive probes for mechanical stress, *Chem. Sci.*, 2016, **7**, 370–375.
7 P. S. Hariharan, V. K. Prasad, S. Nandi, A. Anoop, D. Moon and S. P. Anthony, Molecular Engineering of Triphenylamine Based Aggregation Enhanced Emissive Fluorophore: Structure-Dependent Mechanochromism and Self-Reversible Fluorescence Switching, *Cryst. Growth Des.*, 2017, **17**, 146–155.
8 S. P. Anthony, Organic Solid-State Fluorescence: Strategies for Generating Switchable and Tunable Fluorescent Materials, *ChemPlusChem*, 2012, **77**, 518–531.
9 D. Yan and D. G. Evans, Molecular crystalline materials with tunable luminescent properties: from polymorphs to multi-component solids, *Mater. Horiz.*, 2014, **1**, 46–57.
10 D. Yan, A. Delori, G. O. Lloyd, B. Patel, T. Friščić, G. M. Day, D.-K. Bučar, W. Jones, J. Lu, M. Wei, D. G. Evans and X. Duan, Modification of luminescent properties of a coumarin derivative by formation of multi-component crystals, *CrystEngComm*, 2012, **14**, 5121–5123.
11 D. Yan, A. Delori, G. O. Lloyd, T. Friščić, G. M. Day, W. Jones, J. Lu, M. Wei, D. G. Evans and X. Duan, A Cocrystal Strategy to Tune the Luminescent Properties of Stilbene-Type Organic Solid-State Materials, *Angew. Chem., Int. Ed.*, 2011, **50**, 12483–12486.
12 S. Yagai, T. Seki, H. Aonuma, K. Kawaguchi, T. Karatsu, T. Okura, A. Sakon, H. Uekusa and H. Ito, Mechanochromic Luminescence Based on Crystal-to-Crystal Transformation Mediated by a Transient Amorphous State, *Chem. Mater.*, 2016, **28**, 234–241.
13 H. Zhu, S. Weng, H. Zhang, H. Yu, L. Kong, Y. Zhong, Y. Tian and J. Yang, A novel carbazole derivative containing fluorobenzene unit: aggregation-induced fluorescence emission, polymorphism, mechanochromism and non-reversible thermo-stimulus fluorescence, *CrystEngComm*, 2018, **20**, 2772–2779.
14 Z. He, L. Zhang, J. Mei, T. Zhang, J. W. Y. Lam, Z. Shuai, Y. Q. Dong and B. Z. Tang, Polymorphism-Dependent and Switchable Emission of Butterfly-Like Bis(diarylmethylene)-dihydroanthracenes, *Chem. Mater.*, 2015, **27**, 6601–6607.
15 Y.-X. Li, Z.-F. Yu, C.-Z. Zhu, X.-F. Yang, Y. Nie, Y. Cui and G.-X. Sun, Three new metastable polymorphs of 1-(9-anthryl)-2-(1-naphthyl)ethylene and the polymorph-dependent phase transition and fluorescence change properties, *CrystEngComm*, 2019, **21**, 1512–1518.
16 Y.-X. Li, X.-F. Yang, J.-L. Miao, Z.-W. Zhang and G.-X. Sun, Effects of substitution position on crystal packing, polymorphism and crystallization-induced emission of (9-anthryl)vinylstyrylbenzene isomers, *CrystEngComm*, 2016, **18**, 2098–2104.
17 X. He, A. C. Benniston, H. Saarenpää, H. Lemmetyinen, N. V. Tkachenko and U. Baisch, Polymorph crystal packing effects on charge transfer emission in the solid state, *Chem. Sci.*, 2015, **6**, 3525–3532.
18 Q. Feng, J. Wang, S. Ding, Y. Chen, G. Diao and P. Zhu, Polymorphism and solvates of 1-acetyl-3-(phenyl)-5-(1-pyrenyl)pyrazoline: the structures, thermal and optical-physical properties, *CrystEngComm*, 2018, **20**, 661–667.
19 R. R. Cui, Y. C. Lv, Y. S. Zhao, N. Zhao and N. Li, Solid-state fluorescent materials based on coumarin derivatives: polymorphism, stimuli-responsive emission, self-assembly and optical waveguides, *Mater. Chem. Front.*, 2018, **2**, 910–916.
20 M. Li, Q. Zhang, J.-R. Wang and X. Mei, Mechanochromism triggered fluorescent color switching among polymorphs of a natural fluorescence pigment, *Chem. Commun.*, 2016, **52**, 11288–11291.
21 Z. Zhang, Z. Wu, J. Sun, B. Yao, P. Xue and R. Lu, β-Iminoenolate boron complex with terminal triphenylamine exhibiting polymorphism and mechanofluorochromism, *J. Mater. Chem. C*, 2016, **4**, 2854–2861.
22 F. Borbone, A. Tuzi, B. Panunzi, S. Piotto, S. Concilio, R. Shikler, S. Nabha and R. Centore, On–Off Mechano-responsive Switching of ESIPT Luminescence in Polymorphic N-Salicylidene-4-amino-2-methylbenzotriazole, *Cryst. Growth Des.*, 2017, **17**, 5517–5523.
23 R. Tan, Q. Lin, Y. Wen, S. Xiao, S. Wang, R. Zhang and T. Yi, Polymorphism and mechanochromic luminescence of a highly solid-emissive quinoline-β-ketone boron difluoride dye, *CrystEngComm*, 2015, **17**, 6674–6680.
24 Y. Qi, Y. Wang, Y. Yu, Z. Liu, Y. Zhang, G. Du and Y. Qi, High-contrast mechanochromism and polymorphism-dependent fluorescence of difluoroboron β-diketonate complexes based on the effects of AIEE and halogen, *RSC Adv.*, 2016, **6**, 33755–33762.
25 J. Bernstein, Polymorphism – A Perspective, *Cryst. Growth Des.*, 2011, **11**, 632–650.
26 A. J. Cruz-Cabeza, S. M. Reutzel-Edens and J. Bernstein, Facts and fictions about polymorphism, *Chem. Soc. Rev.*, 2015, **44**, 8619–8635.
27 A. Nangia, Conformational Polymorphism in Organic Crystals, *Acc. Chem. Res.*, 2008, **41**, 595–604.
28 A. G. Dikundwar, G. K. Dutta, T. N. Guru Row and S. Patil, Polymorphism in Opto-Electronic Materials with a Benzothiazole-fluorene Core: A Consequence of High Conformational Flexibility of π-Conjugated Backbone and Alkyl Side Chains, *Cryst. Growth Des.*, 2011, **11**, 1615–1622.
29 P. S. Hariharan, M. B. Mariyatra, E. M. Mothi, A. Neels, G. Rosair and S. P. Anthony, Polymorphism and benzene solvent controlled stimuli responsive reversible fluorescence switching in triphenylphosphoniumfluorenylide crystals, *New J. Chem.*, 2017, **41**, 4592–4598.
30 P. Gayathri, M. Pannipara, A. G. Al-Sehemi and S. P. Anthony, Triphenylamine-based stimuli-responsive solid state fluorescent materials, *New J. Chem.*, 2020, **44**, 8680–8696.
31 D. Tchoń, D. Trzybiński, A. Wrona-Piotrowicz and A. Makal, Polymorphism and resulting luminescence properties of 1-acetylpyrene, *CrystEngComm*, 2019, **21**, 5845–5852.
32 X. Ma, J. Cheng, J. Liu, X. Zhou and H. Xiang, Ratiometric fluorescent pH probes based on aggregation-induced emission-active salicylaldehyde azines, *New J. Chem.*, 2015, **39**, 492–500.

33 P. S. Hariharan, D. Moon and S. P. Anthony, Reversible fluorescence switching and topochemical conversion in an organic AEE material: polymorphism, defection and nanofabrication mediated fluorescence tuning, *J. Mater. Chem. C*, 2015, **3**, 8381–8388.

34 P. S. Hariharan, G. Parthasarathy, A. Kundu, S. Karthikeyan, Y. Sagara, D. Moon and S. P. Anthony, Drastic Modulation of Stimuli-Responsive Fluorescence by a Subtle Structural Change of Organic Fluorophore and Polymorphism Controlled Mechanofluorochromism, *Cryst. Growth Des.*, 2018, **18**, 3971–3979.

35 P. Gayathri, S. Karthikeyan, M. Pannipara, A. G. Al-Sehemi, D. Moon and S. P. Anthony, Aggregation-enhanced emissive mechanofluorochromic carbazole-halogen positional isomers: tunable fluorescence via conformational polymorphism and crystallization-induced fluorescence switching, *CrystEngComm*, 2019, **21**, 6604–6612.

36 Z. Lin, X. Mei, E. Yang, X. Li, H. Yao, G. Wen, C.-T. Chien, T. J. Chow and Q. Ling, Polymorphism-dependent fluorescence of bisthienylmaleimide with different responses to mechanical crushing and grinding pressure, *CrystEngComm*, 2014, **16**, 11018–11026.

37 G. Huang, Y. Jiang, S. Yang, B. S. Li and B. Z. Tang, Multistimuli Response and Polymorphism of a Novel Tetraphenylethylene Derivative, *Adv. Funct. Mater.*, 2019, **29**, 1900516.

38 Y. Chen, X. Zhang, M. Wang, J. Peng, Y. Zhou, X. Huang, W. Gao, M. Liu and H. Wu, Mechanofluorochromism, polymorphism and thermochromism of novel D–π–A piperidin-1-yl-substitued isoquinoline derivatives, *J. Mater. Chem. C*, 2019, **7**, 12580–12587.

39 X. Zhang, J. Wang, Y. Liu, Y. Hao, F. Yu, D. Li, X. Huang, L. Yu, T. Wang and H. Hao, Tunable Emission of Organic Fluorescent Crystals through Polymorphic Manipulation, *J. Phys. Chem. C*, 2021, **125**, 6189–6199.

40 S. Ito, Luminescent polymorphic crystals: mechanoresponsive and multicolor-emissive properties, *CrystEngComm*, 2022, **24**, 1112–1126.

41 S. W. Thomas, G. D. Joly and T. M. Swager, Chemical Sensors Based on Amplifying Fluorescent Conjugated Polymers, *Chem. Rev.*, 2007, **107**, 1339–1386.

42 T. Jadhav, B. Dhokale, Y. Patil, S. M. Mobin and R. Misra, Multi-Stimuli Responsive Donor–Acceptor Tetraphenylethylene Substituted Benzothiadiazoles, *J. Phys. Chem. C*, 2016, **120**, 24030–24040.

43 J. Luo, Z. Xie, J. W. Y. Lam, L. Cheng, H. Chen, C. Qiu, H. S. Kwok, X. Zhan, Y. Liu, D. Zhu and B. Z. Tang, Aggregation-induced emission of 1-methyl-1,2,3,4,5-pentaphenylsilole, *Chem. Commun.*, 2001, 1740–1741.

44 J. Mei, Y. Hong, J. W. Y. Lam, A. Qin, Y. Tang and B. Z. Tang, Aggregation-Induced Emission: The Whole Is More Brilliant than the Parts, *Adv. Mater.*, 2014, **26**, 5429–5479.

45 Y. Hong, J. W. Y. Lam and B. Z. Tang, Aggregation-induced emission: phenomenon, mechanism and applications, *Chem. Commun.*, 2009, 4332–4353.

46 J. Chen, B. Xu, X. Ouyang, B. Z. Tang and Y. Cao, Aggregation-Induced Emission of cis,cis-1,2,3,4-Tetraphenylbutadiene from Restricted Intramolecular Rotation, *J. Phys. Chem. A*, 2004, **108**, 7522–7526.

47 S. Choi, J. Bouffard and Y. Kim, Aggregation-induced emission enhancement of a meso-trifluoromethyl BODIPY via J-aggregation, *Chem. Sci.*, 2014, **5**, 751–755.

48 M. Zhang, W. Yang, T. Gong, W. Zhou and R. Xue, Tunable AIEE fluorescence constructed from a triphenylamine luminogen containing quinoline – application in a reversible and tunable pH sensor, *Phys. Chem. Chem. Phys.*, 2017, **19**, 21672–21682.

49 J. Mei, N. L. C. Leung, R. T. K. Kwok, J. W. Y. Lam and B. Z. Tang, Aggregation-Induced Emission: Together We Shine, United We Soar!, *Chem. Rev.*, 2015, **115**, 11718–11940.

50 R. T. K. Kwok, C. W. T. Leung, J. W. Y. Lam and B. Z. Tang, Biosensing by luminogens with aggregation-induced emission characteristics, *Chem. Soc. Rev.*, 2015, **44**, 4228–4238.

51 J. Zhao, Z. Chi, Z. Yang, Z. Mao, Y. Zhang, E. Ubba and Z. Chi, Recent progress in the mechanofluorochromism of distyrylanthracene derivatives with aggregation-induced emission, *Mater. Chem. Front.*, 2018, **2**, 1595–1608.

52 H. Liu, Z. Lu, B. Tang, Z. Zhang, Y. Wang and H. Zhang, AIE-active organic polymorphs displaying molecular conformation-dependent amplified spontaneous emissions (ASE), *Dyes Pigm.*, 2018, **149**, 284–289.

53 Z. Yang, Z. Chi, Z. Mao, Y. Zhang, S. Liu, J. Zhao, M. P. Aldred and Z. Chi, Recent advances in mechano-responsive luminescence of tetraphenylethylene derivatives with aggregation-induced emission properties, *Mater. Chem. Front.*, 2018, **2**, 861–890.

54 P. Sarma, K. Patir, K. K. Sarmah, S. K. Gogoi, R. Thakuria and P. J. Das, Stimuli-responsive aggregation-induced fluorescence in a series of biphenyl-based Knoevenagel products: effects of substituent active methylene groups on [pi]-[pi] interactions, *Acta Crystallogr., Sect. B: Struct. Sci., Cryst. Eng. Mater.*, 2019, **75**, 775–783.

55 P. Sarma, K. K. Sarmah, D. Kakoti, S. P. Mahanta, N. M. Adassooriya, G. Nandi, P. J. Das, D.-K. Bučar and R. Thakuria, A readily accessible porous organic polymer facilitates high-yielding Knoevenagel condensation at room temperature both in water and under solvent-free mechanochemical conditions, *Catal. Commun.*, 2021, **154**, 106304.

56 J. W. Bridges, P. J. Creaven and R. T. Williams, The fluorescence of some biphenyl derivatives, *Biochem. J.*, 1965, **96**, 872–878.

57 J. Sturala, M. K. Etherington, A. N. Bismillah, H. F. Higginbotham, W. Trewby, J. A. Aguilar, E. H. C. Bromley, A.-J. Avestro, A. P. Monkman and P. R. McGonigal, Excited-State Aromatic Interactions in the Aggregation-Induced Emission of Molecular Rotors, *J. Am. Chem. Soc.*, 2017, **139**, 17882–17889.

58 Y. Zhou, L. Qian, M. Liu, G. Wu, W. Gao, J. Ding, X. Huang and H. Wu, The influence of different N-substituted groups on the mechanochromic properties of 1,4-dihydropyridine

derivatives with simple structures, *RSC Adv.*, 2017, **7**, 51444–51451.
59 F. Yu, M. Wang, H. Sun, Y. Shan, M. Du, A. Khan, R. Usman, W. Zhang, H. Shan and C. Xu, Tuning the solid-state fluorescence of chalcone crystals via molecular coplanarity and J-aggregate formation, *RSC Adv.*, 2017, **7**, 8491–8503.
60 S. Hisamatsu, H. Masu, M. Takahashi, K. Kishikawa and S. Kohmoto, Pairwise Packing of Anthracene Fluorophore: Hydrogen-Bonding-Assisted Dimer Emission in Solid State, *Cryst. Growth Des.*, 2015, **15**, 2291–2302.
61 M. A. Spackman and D. Jayatilaka, Hirshfeld surface analysis, *CrystEngComm*, 2009, **11**, 19–32.
62 M. Turner, J. McKinnon, S. Wolff, D. Grimwood, P. Spackman, D. Jayatilaka and M. Spackman, *CrystalExplorer17*, The University of Western Australia Perth, WA, Australia, 2017.
63 D. Dey, S. P. Thomas, M. A. Spackman and D. Chopra, 'Quasi-isostructural polymorphism' in molecular crystals: inputs from interaction hierarchy and energy frameworks, *Chem. Commun.*, 2016, **52**, 2141–2144.